Electronic Supplementary Material (ESI) for RSC Advances.

Supplementary Information:

Insights into the spontaneous formation of hybrid PdO_x/PEDOT films: electroless deposition and oxygen reduction activity

Julian A. Vigil,[a] *Michael T. Brumbach,*[b] *Jonathon Duay,*[a] *and Timothy. N. Lambert**[a]

[a] Department of Materials, Devices & Energy Technologies, Sandia National Laboratories, Albuquerque, New Mexico 87185, USA.

[b] Materials Characterization & Performance, Sandia National Laboratories, Albuquerque, New Mexico 87185, USA.

* E-mail: tnlambe@sandia.gov; Tel.: +1 505 284 6967.

Table of Contents:

Characterization Methods:

Electrochemical Characterization. r-PEDOT and PdO_x/PEDOT films were deposited on the disk of GC disk/Au ring rotating ring disk working electrodes (disk area = 0.2475 cm^2, ring area = 0.1866 cm^2; Pine Research Instrumentation) and transferred to a three-electrode cell directly from the water bath following the preparation described above. The r-PEDOT or PdO_x/PEDOT working electrode was accompanied by a graphite rod counter electrode and standard calomel reference electrode (sat. KCl, +0.244 V vs. NHE; Hach). All experiments were carried out in a glass cell, controlled by the MSR rotator unit and WaveDriver 20 Bipotentiostat (Pine Research Instrumentation).

For cyclic voltammetry (CV) studies, the potential of the working electrode was cycled at a scan rate of 50 mV s^{-1} (beginning in the cathodic direction) with no rotation in 0.1 M KOH. The electrolyte was bubbled with pure Ar or O_2 gas as noted for 20 min. prior to the experiment and blanketed throughout. For comparative CV studies in the presence of O_2, the films were cycled 10 times in Ar prior to bubbling the electrolyte with O_2 and proceeding with the same film. The active electrochemical surface area (ECSA) of Pd species on the PdO_x/PEDOT electrode was calculated using the integral area of the oxide reduction wave ($E_p \approx 0.6$ V vs. RHE) in the CV according to Eq. S1 and Eq. S2,

$$Q = \frac{1}{\upsilon}\int_{E_1}^{E_2} I dE \tag{S1}$$

$$ECSA = \frac{Q}{Q_r} \tag{S2}$$

where Q is charge, ν is scan rate, E is potential, and I is current. A standard reference value (Q_r) of 0.42 mC cm^{-2} is used for the charge density associated with a monolayer coverage of O on Pd.[1]

The oxygen reduction reaction (ORR) activity of PEDOT, PdO_x/PEDOT, and commercial 20% Pt/C was investigated by linear scanning voltammetry (LSV) using hydrodynamic rotating ring disk electrode (RRDE) methods. The PEDOT and PdO_x/PEDOT electrodes were used directly in the cell as described above. 20% Pt/C films were prepared by drop-casting a 10 μL aliquot of

catalyst ink (2.5 mg 20% Pt/C:0.75 mL DI H_2O:0.2 mL IPA:0.05 mL Nafion soln.) after 20 min sonication on the polished disk of the working electrode (mass loading = 101 μg cm^{-2} = 20 μg_{Pt} cm^{-2}). LSV scans were completed at a rate of 10 mV s^{-1}, scanning from 0.2 to -1.0 V vs. SCE in a sequence with increasing rotation rates: 400, 900, 1600, 2500, 3600 RPM. The 0.1 M KOH electrolyte was bubbled with pure Ar or O_2 gas prior for 20 min. prior to the respective experiment and blanketed throughout. For each set of LSV scans, background current measured in O_2-free (Ar) environment was subtracted from the corresponding catalytic current in the presence of O_2 prior to analysis. Half-wave potential ($E_{1/2}$) was calculated using limiting current density defined as the measured disk current at 0.2 V vs. RHE; onset potential was calculated using the tangential method, as previously reported.[2] The collection efficiency (N) of the RRDE GC/Au working electrode was determined to be 0.36 using the $[Fe(CN)_6]^{3-/4-}$ couple. The ORR electron transfer number (n) and fraction of peroxide generation (f_p) were calculated from the background-subtracted disk current (i_d) and ring current (i_r) according to Eq. S3 and Eq. S4, respectively:

$$n = \frac{4*i_d}{\frac{i_r}{N}+i_d} \tag{S3}$$

$$f_p = \frac{2*\frac{i_r}{N}}{\frac{i_r}{N}+i_d} \tag{S4}$$

n and the kinetic rate constant (k) were also calculated using Koutecky-Levich (K-L) analysis with the ORR LSVs recorded at each rotation rate. The slope and intercept of linear fits of the K-L plots (inverse current vs. inverse square root of the rotation rate) from 0.2 V to 0.7 V vs. RHE were used to solve the K-L equation,

$$\frac{1}{j} = \frac{1}{j_{lim}} + \frac{1}{j_k} = \frac{1}{0.62nFC_0(D_0)^{\frac{2}{3}}\nu^{-\frac{1}{6}}\omega^{\frac{1}{2}}} + \frac{1}{nFkC_0} \tag{S5}$$

where j is current density, j_{lim} is limiting current density, j_k is kinetic current density, F is the Faraday constant (96485 C mol^{-1}), C_0 is the concentration of dissolved O_2 (1.2 x 10^{-6} mol cm^{-3}), D_0 is the diffusion coefficient of O_2 (1.9 x 10^{-5} cm^2 s^{-1}), ν is the kinematic viscosity of the electrolyte (1.1 x 10^{-2} cm^2 s^{-1}), and ω is the rotation rate.[3] ORR kinetic current (i_k) was calculated using a limiting current (i_{lim}) value taken at 0.2 V vs. RHE from the background-subtracted i_d at 2500 RPM according to Eq. S6:

$$i_k = \frac{i_d * i_{lim}}{i_{lim} - i_d} \quad \text{(S6)}$$

Specific j_k was calculated from i_k using the ECSA (1.05 cm^2) and average mass loading (3.185 μg) of Pd species from CV studies and combined quartz crystal microbalance/elemental analysis, respectively.

Stability of the 20% Pt/C and PdO_x/PEDOT electrodes was assessed by electrolysis at 0.8 V vs. RHE for 3 h at 2500 RPM. The 0.1 M KOH electrolyte was gently purged with O_2 throughout the experiment. The first five minutes of CPE was used as equilibration time for the electrode, thus i at t = 5 min was used as initial current (i_0) in measuring the chronoamperometric response.

Quartz Crystal Microbalance (QCM) Measurements. The mass of the film was monitored during electropolymerization and electroless deposition of Pd using a Maxtek RQCM Quartz Crystal Microbalance Research System (Inficon) with the three-electrode cell and Solartron 1287 Potentiostat described above. A 1 in. AT-Cut, 9 MHz Ti/Pt quartz crystal (Inficon) cleaned with detergent, dried under Ar flow, and housed in a CHK-100 Kynar® crystal holder (Inficon) acted as the working electrode and piezoelectric sensing crystal. The intrinsic capacitance of the crystal assembly and connection to the instrument were accounted for by cancellation while submerged in CH_3CN prior to each measurement (no significant change in capacitance was observed upon transferring the crystal from CH_3CN to aqueous solutions). For QCM studies, a 60-s open circuit potential (OCP) segment was added prior to the electropolymerization procedure, which otherwise proceeded as described above. The mass change associated with electroless deposition was normalized to the minimum mass reached within 60 s after being transferred to the aqueous deposition solution, which signaled the onset of Pd uptake. Mass change (Δm) was calculated from measured crystal frequency change (Δf) according to the Sauerbrey Equation (Eq. S7),

$$\Delta f = -\frac{2nf_0^2}{\sqrt{\rho_q \mu_q}} \Delta m = -C_f \Delta m \quad \text{(S7)}$$

where n is the harmonic number, f_0 is the resonant frequency, ρ_q is the density of quartz, and μ_q is the shear modulus of the quartz crystal, which simplify to the sensitivity factor, C_f (0.1834 Hz ng^{-1} cm^{-2} for the 9 MHz crystal used here at 20 °C).

X-Ray Photoelectron Spectroscopy (XPS). X-ray photoelectron spectroscopy was performed with a Kratos AXIS Supra instrument. Base pressures were less than $5 \cdot 10^{-9}$ Torr. Excitation was from a monochromatic Al Kα (1486.7 eV) X-ray source operating at 75 W for survey spectra at 160 eV pass energy. For high resolution spectra, the X-ray source was operated at 150 W and a 20 eV pass energy was utilized. The analyzed spot was an elliptical area of 300 x 700 microns. The sample electrodes were grounded, however, to compensate for differential charging effects, charge neutralization was achieved using low energy electrons supplied from a filament above the sample. Data analysis was performed in CasaXPS.

Inductively Coupled Plasma Mass Spectrometry (ICP-MS) Measurements. Approximately 300 mg PdO_x/PEDOT samples deposited on a GC electrode (on SiO_2) were removed from the electrode and digested in fresh aqua regia (1 mol HNO_3: 3 mol HCl). The digested solutions were then diluted 100-fold with 2% nitric acid. The diluted solutions, along with palladium standard solutions, were analyzed using a NexION 350D ICP-MS instrument (Perkin Elmer) utilizing germanium as an internal standard.

Scanning Electron Microscopy/Energy Dispersive Spectroscopy (SEM/EDS). r-PEDOT and PEDOT/PdO_x films were deposited on GC electrodes on SiO_2 substrates. High resolution SEM imaging was performed on a FEI Nova 600 Nanolab field emission source microscope using a through lens detector. EDS mapping was acquired on a Tescan Vega-3 LMU Tungsten Filament microscope using a TEAM EDAX Analysis System. All samples were sputter coated with platinum prior to SEM/EDS analysis.

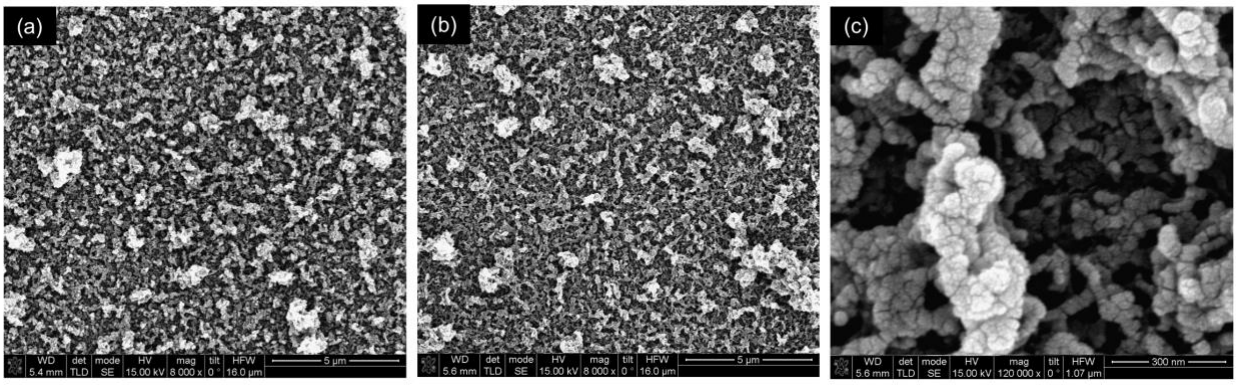

Fig. S1 SEM images of a PdO_x/PEDOT film in low magnification (a) and a r-PEDOT film in low (b) and high (c) magnification.

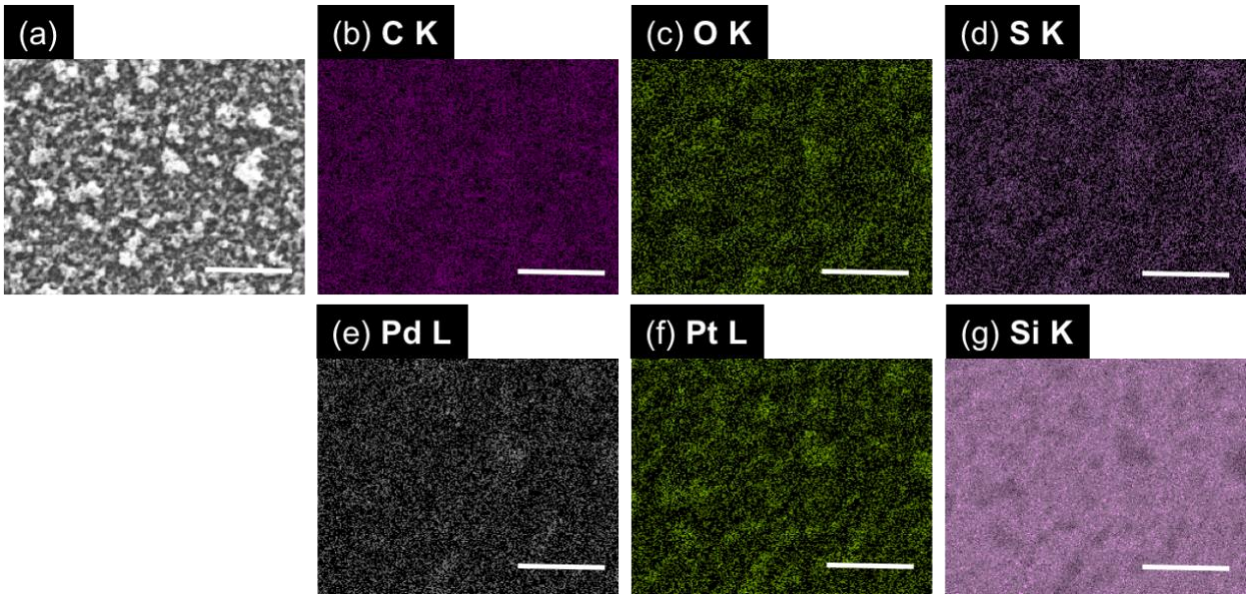

Fig. S2 SEM and EDS elemental mapping of a PdO_x/PEDOT film as-deposited on a GC electrode. Pt and Si content are attributed to sputter coating and the electrode substrate, respectively.

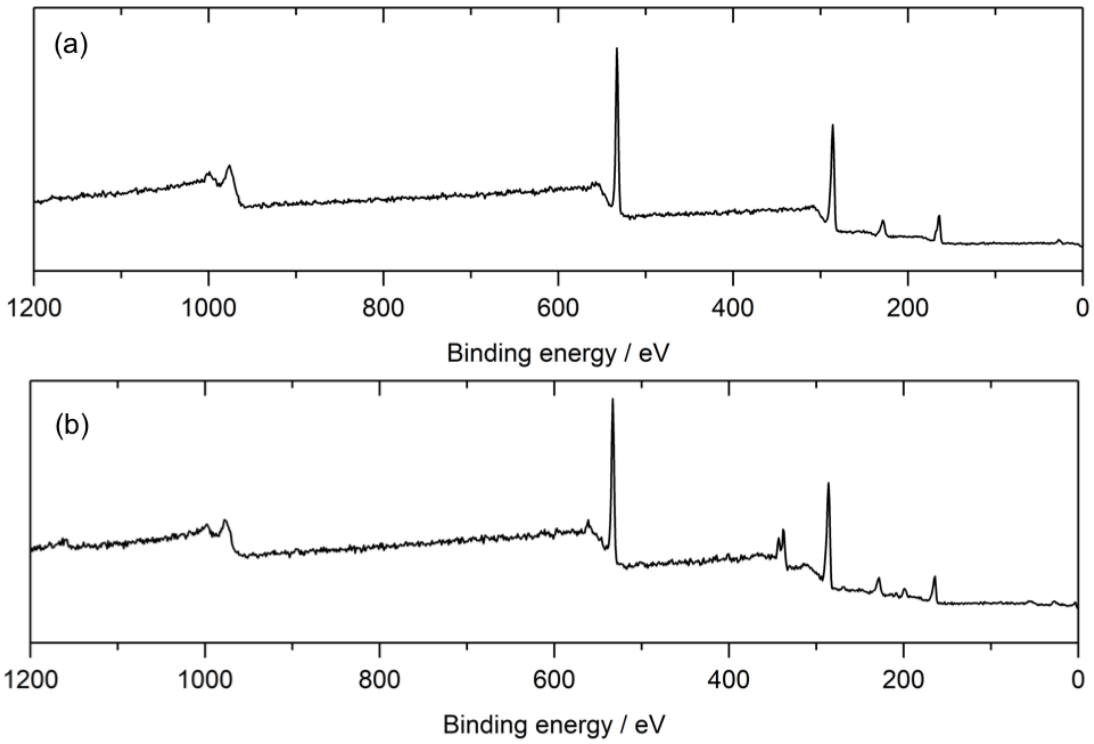

Fig. S3 Representative XPS survey spectra for the r-PEDOT (a) and PdO_x/PEDOT (b) films as-deposited on GC electrodes.

Table S1 Binding Energies and Fit FWHM for Pd 3d, O 1s, C 1s and S 2p Core Level Electron Peaks Measured by XPS

	BE (eV) r-PEDOT	FWHM r-PEDOT	BE (eV) PdO_x/PEDOT	FWHM PdO_x/PEDOT
Pd 3d	*	*	336.02 ± 0.15 337.78 ± 0.05 338.77 ± 0.14 341.15 ± 0.10 343.04 ± 0.05 344.50 ± 0.17	1.47 ± 0.12 1.38 ± 0.12 1.60 1.47 ± 0.12 1.38 ± 0.12 1.60
O 1s	531.74 ± 0.02 533.30 ± 0.01 535.00	1.62 ± 0.04 1.59 ± 0.01 2.00 ± 0.01	531.71 ± 0.06 533.30 ± 0.02 535.00 536.91 ± 0.09	1.69 ± 0.05 1.64 ± 0.04 1.98 ± 0.05 1.87 ± 0.15
C 1s	285.00 286.52 ± 0.01 288.70 ± 0.04	1.11 ± 0.01 1.67 ± 0.01 2.39 ± 0.05	285.00 286.45 ± 0.02 288.60 ± 0.09	1.14 ± 0.03 1.65 ± 0.05 2.57 ± 0.18
S 2p	164.01 ± 0.01 164.95 ± 0.03 165.47 ± 0.01 166.24 ± 0.01 167.77 ± 0.03 169.19 ± 0.09	0.85 ± 0.01 0.85 ± 0.01 0.92 ± 0.03 0.92 ± 0.03 2.00 2.00	163.99 ± 0.03 164.97 ± 0.04 165.47 ± 0.03 166.31 ± 0.04 167.50 ± 0.01 169.03 ± 0.05	0.91 ± 0.02 0.91 ± 0.02 1.00 1.00 1.80 ± 0.15 1.80 ± 0.15

* = not detected

Table S2 Atomic Concentrations from XPS Core Level Fits (At. %)

	C	Cl	N	O	S	Pd
r-PEDOT	62.2 ± 0.7	*	1.0 ± 0.1	30.5 ± 0.7	6.28 ± 0.2	*
PdO_x/PEDOT	57 ± 2	2.2 ± 0.5	1.7 ± 0.4	31 ± 1	5.5 ± 0.4	3.0 ± 0.8

* = not detected

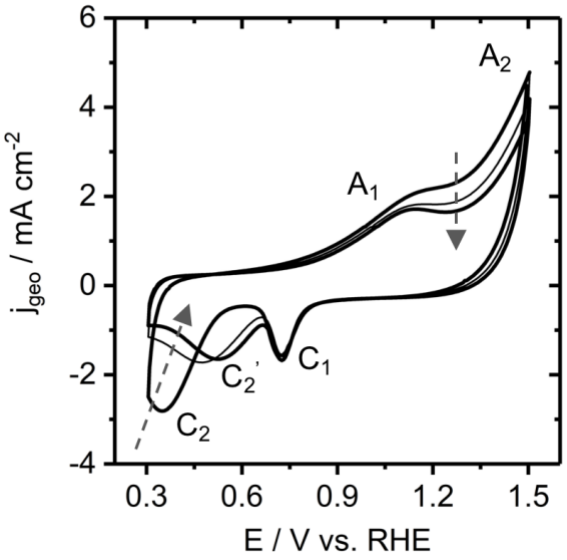

Fig. S4 CV scans of the PdO_x/PEDOT film on GC in Ar-saturated 0.1 M KOH with anodic switching potential of 1.5 V vs. RHE. See main text for assignment and discussion of the C_1/A_1 and C_2 processes (Fig. 1c). Extending the anodic switching potential to 1.5 V vs. RHE results in the onset of irreversible anodic current at ~1.4 V vs. RHE (A_2), corresponding to concomitant oxygen evolution and oxidation of Pd to Pd^{4+}.[4] In the cathodic scan, C_1 is shifted positive to 0.7 V vs. RHE, and the C_2 wave is again observed at 0.3 V vs. RHE in the first scan and stabilizes at a potential of 0.5 V vs. RHE in subsequent cycles (C_2').

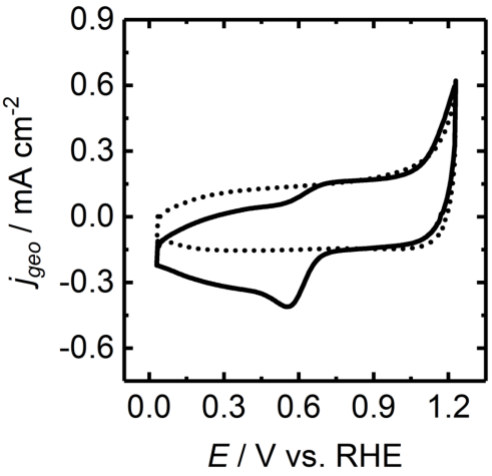

Fig. S5 CV scans of a r-PEDOT film deposited on a GC RRDE electrode in Ar-saturated (dotted line) and O_2-saturated (solid line) 0.1 M KOH.

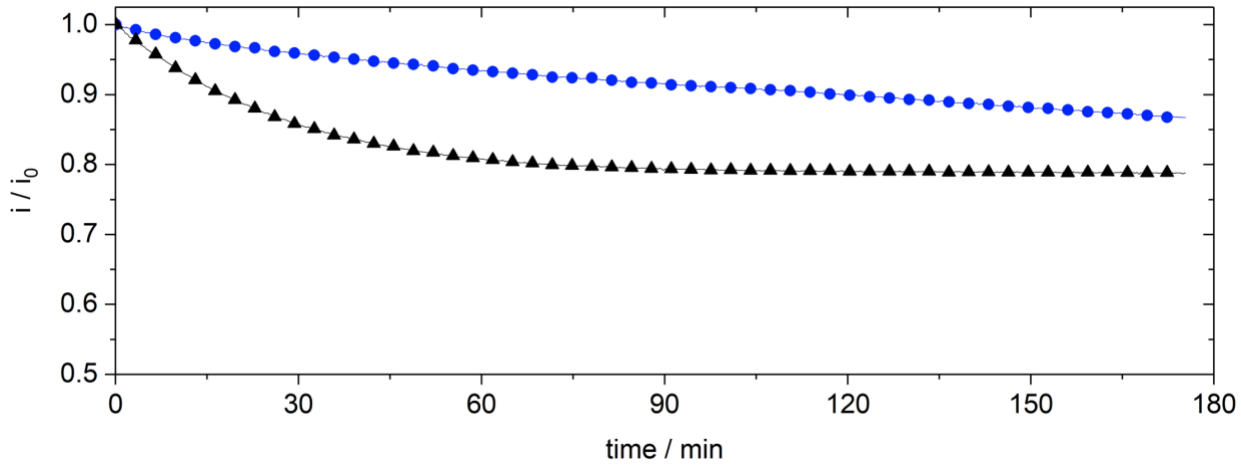

Fig. S6 Chronoamperometric response of the PdO_x/PEDOT (blue circles) and 20% Pt/C (black triangles) films during controlled potential electrolysis at 0.8 V vs. RHE in continuously O_2-purged 0.1 M KOH electrolyte for three hours.

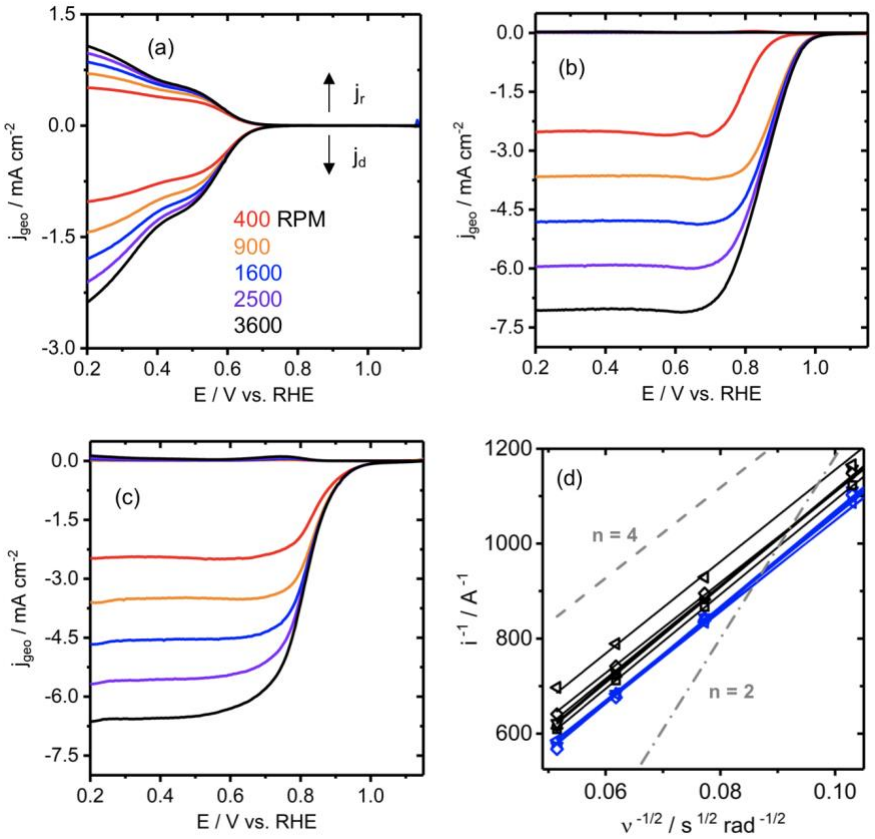

Fig. S7 ORR LSVs (ring and disk current densities) measured by RRDE at increasing rotation rates from 400 RPM to 3600 RPM in 0.1 M KOH electrolyte for the r-PEDOT (a), PdO_x/PEDOT (b), and 20% Pt/C (c) films; (d) Koutecky-Levich plots and linear fits for PdO_x/PEDOT (blue) and 20% Pt/C (black) over the potential range of 0.2 V to 0.7 V vs. RHE and example slopes corresponding with n = 2 and n = 4 ORR processes.

Table S3 ORR Activity Comparison with Relevant Literature Reports on Pd-based Electrocatalysts in 0.1 M KOH

	Ref.	E_{onset} / V vs. RHE	$E_{1/2}$ / V vs. RHE	j_k / mA cm^{-2}_{ECSA}	j_k / mA μg^{-1}_{Pd}	n / e^-
PdO_x/PEDOT	this work	0.98	0.86	6.03 [a] 1.93 [b] 0.65 [c]	1.99 [a] 0.64 [b] 0.22 [c]	3.97
Pd/C-AR	3	NR	NR	0.14 [c]	0.08 [c]	3.9
Pd/C-300				0.17 [c]	0.09 [c]	3.7
Pd/C-400				0.2 [c]	0.10 [c]	3.9
Pd/C-500				0.23 [c]	0.07 [c]	3.7
Pd/C-600				0.39 [c]	0.05 [c]	3.9
PdO/C-0.5h	5	0.95	0.84	2.00 [b]	0.15 [b]	3.8-3.96
PdO/C-1h		0.96	0.85	2.69 [b]	0.18 [b]	3.88-3.97
PdO/C-2h		0.99	0.90	1.40 [b]	0.36 [b]	3.92-3.97
PdO/C-4h		1.0	0.92	2.64 [b]	1.11 [b]	3.91-3.99
PdO/C-8h		1.0	0.92	1.27 [b]	0.72 [b]	3.91-3.99
PdSph-20	6	NR	NR	0.15 ± 0.08 [c]	0.10 ± 0.01 [c]	NR
PdCub3-20				0.37 ± 0.10 [c]	0.09 ± 0.02 [c]	
PdCub2-20				0.42 ± 0.05 [c]	0.06 ± 0.01 [c]	
PdCub1-50				0.50 ± 0.08 [c]	0.04 ± 0.01 [c]	
PdCub1-20				0.55 ± 0.08 [c]	0.06 ± 0.01 [c]	
Pd/CNS-10%	7	0.91	NR	0.11 [d]	0.17 [d]	
Pd/CNS-15%		0.92		0.13 [d]	0.2 [d]	
Pd/CNS-20%		0.96		0.16 [d]	0.29 [d]	3.86-3.98
Pd/CNS-25%		0.93		0.12 [d]	0.22 [d]	
Pd/PEDOT/rGO	8	0.98	NR	~3.25 [a]	~1.2 [a]	3.7

[a] 0.8 V vs. RHE, [b] 0.85 V vs. RHE, [c] 0.9 V vs. RHE, [d] potential not specified.

References

1. M. Łukaszewski, M. Soszko and A. Czerwiński, *Int. J. Electrochem. Sci.*, 2016, **11**, 4442-4469.
2. D. J. Davis, T. N. Lambert, J. A. Vigil, M. A. Rodriguez, M. T. Brumbach, E. N. Coker and S. J. Limmer, *J. Phys. Chem. C*, 2014, **118**, 17342-17350.
3. L. Jiang, A. Hsu, D. Chu and R. Chen, *J. Electrochem. Soc.*, 2009, **156**, B643-B649.
4. M. Grdeń, M. Łukaszewski, G. Jerkiewicz and A. Czerwiński, *Electrochim. Acta*, 2008, **53**, 7583-7598.
5. Q. Wu, Z. Rao, L. Yuan, L. Jiang, G. Sun, J. Ruan, Z. Zhou and S. Sang, *Electrochim. Acta*, 2014, **150**, 157-166.
6. M. Lüsi, H. Erikson, A. Sarapuu, K. Tammeveski, J. Solla-Gullón and J. M. Feliu, *Electrochem. Commun.*, 2016, **64**, 9-13.
7. W. Yan, Z. Tang, L. Li, L. Wang, H. Yang, Q. Wang, W. Wu and S. Chen, *ChemElectroChem*, 2017, **4**, 1349-1355.
8. J. E. Choe, M. S. Ahmed and S. Jeon, *J. Power Sources*, 2015, **281**, 211-218.